Received: 6 October 2021 | Revised: 20 November 2021 | Accepted: 26 November 2021

DOI: 10.1002/pat.5574

RESEARCH ARTICLE

polymers advanced technologies WILEY

Plasmonic enhanced polymer solar cell with inclusion of $Ag@SiO_2$ core-shell nanostructures

Elmira Alikhaidarova[1] | Dmitriy Afanasyev[1,2] | Niyazbek Ibrayev[1] | Nurxat Nuraje[3,4]

[1]Institute of Molecular Nanophotonics, Buketov Karaganda University, Karaganda, Kazakhstan

[2]Institute of Applied Mathematics, Karaganda, Kazakhstan

[3]Department of Chemical and Materials Engineering, School of Engineering and Digital Science, Nazarbayev University, Nur-Sultan, Kazakhstan

[4]Advanced Solar Energy Materials & Systems Lab, National Laboratory Astana, Nur-Sultan, Kazakhstan

Correspondence
Elmira Alikhaidarova, Institute of Molecular Nanophotonics, Buketov Karaganda University, 28, Universitetskaya St., 100028 Karaganda, Kazakhstan.
Email: alikhaidarova@mail.ru

Nurxat Nuraje, Department of Chemical and Materials Engineering, School of Engineering and Digital Science, Nazarbayev University, Nur-Sultan, Kazakhstan.
Email: nurxat.nuraje@nu.edu.kz

Funding information
Nazarbayev University, Grant/Award Number: SEDS2020 016

Abstract

In this work, the effect of $Ag@SiO_2$ core-shell nanostructure (NS) on photovoltaic characteristics of polymer solar cell has been studied. Addition of $Ag@SiO_2$ nanostructure containing SiO_2 dielectric shell into the polymer solar cell eliminates the influence of metal nanoparticles (NP) to electron transfer between the polymer and the metal nanoparticles. The efficiency of the polymer solar cell was increased by 60% for the optimal concentration of $Ag@SiO_2$ NSs (10^{-8} mol/L) in the PEDOT:PSS film. The increased efficiency of the polymer solar cell with inclusion of $Ag@SiO_2$ nanostructure in PEDOT:PSS film was ascribed to a decrease of the electrical resistance of the PEDOT:PSS layer and enhancement of light harvesting by light scattering of $Ag@SiO_2$ nanostructure in the polymer solar cell. The mechanism and kinetics of the plasmonic enhanced polymer solar cell were explained by IPCE, time-resolved photoluminescence spectroscopy, and EIS studies.

KEYWORDS
electrical conductivity, plasmon resonance, polymer solar cells, silicon dioxide, silver nanoparticle

1 | INTRODUCTION

Polymer solar cell (PSC) is currently considered as one of the promising research areas due to its unique advantages such as cost-effectiveness, easy fabrication, and flexible solar panel. The production of the PSC is relatively cheap since it does not require the extreme conditions (high vacuum or clean room) and the roll-to-roll printing technique can be readily adapted to produce them at the large scale. Manufacturing of the PSC is environmentally-benign process.[1] In recent years, due to the discovery of the new promising semiconductor polymers and organic molecules, the high efficiency of polymer solar cells has reached.[2]

Despite the above results achieved by developing the new compounds with excellent optical and electrical characteristics, there are also another viable way to enhance the PSCs efficiency.[3] Furthermore, inclusion of nanoparticles (NPs) and nanostructures (NSs) of metals with pronounced localized surface plasmon resonance (LSPR) is widely explored for the PSCs. Metal NPs have attracted great attention of researchers due to their distinctive properties and potential applications in various fields,[4–7] such as photocatalysis,[8,9] nonlinear optics,[10,11] and optical sensors.[12] Advances in synthesis methods have made it possible to synthesize predicted shapes and sizes of the NPs and NSs.[13–15] Their core-shell NSs have also been successfully synthesized.[15]

Polymer nanocomposites[16–19] of semiconductor materials with inclusion of NPs and NSs have been actively explored due to their application in photovoltaic cells.[20,21] Such nanocomposites have remarkable properties, not typical for intrinsic semiconducting polymers. They are used as essential elements of organic electronics,[22] and as a model system for studying the processes of light conversion into electrical energy in PSC.[23]

Most studies have shown that the addition of NPs into various functional layers leads to an increase in the PSCs efficiency.[20,24]

However, the efficiency of the PSC with addition of plasmon NPs shows different results. The substantial enhancement in the efficiency has been usually observed for the cell with the relatively low efficiency.[24] Often, the increase or decrease of the PSC efficiency is determined by the conducting properties of semiconducting polymers.[25] Sometimes, addition of NPs to the active layer of the cell decreases the efficiency due to the increase of recombination.[20] One of the promising ways to reduce the influence of NPs on the electrical properties is to use metal NPs with a protective shell.[26,27] Oxide materials such as TiO_2 and SiO_2 are often used for shell[26–28] because they possess relatively high stability and dielectric property. Methods for the synthesis of such shell with an accuracy of up to units of nanometers have been developed.

Despite large number of works published on improving the efficiency of PSC with plasmonic NP, there is no unified opinion about enhancement mechanism of its efficiency.[20,21,23] There are a number of mechanisms proposed for the influence of NPs on the light conversion process in PSC:

1. Addition of metal NPs can change the conductivity of semiconducting polymer, thus improve their electrical transport properties[29];
2. Presence of LSPR can lead to an increase in the absorption and scattering of light in polymer films.

Recently, the studies indicate that LSPR can increase the rate of exciton dissociation and reduce the rate of exciton recombination and/or a number of radiative and non-radiative processes.[20] There is also a significant effect of silver NPs on the structure of the polymer film,[30] which will lead to significant improvement on the photovoltaic properties of PSC.

Nanostructures consisting of a dielectric shell (silicon dioxide) around the metal core have advantage over other types of core-shell materials.[15] This is due to their high temperature resistance, colloidal stability, dielectric property, and water compatibility.

Thus, this research work conducted fundamental investigation on the PSC performance through adding the core-shell NSs (consisting of the metal core [Ag] and the dielectric shell of SiO_2) into the conducting polymer film layer based on the hypothesis that: (1) addition of the $Ag@SiO_2$ makes it possible to significantly reduce the effect of these additives on the electrical conductivity of the films or recombination of photogenerated holes/electrons, and (2) increase its optical property. At the same time, we also investigated the mechanism of the LSPR influence on the optical and electrical properties of PSCs. Furthermore, this paper discussed the results from the studies of the $Ag@SiO_2$ nanostructure effect on the efficiency of conversion light into electrical energy in P3HT:PCBM solar cells.

2 | MATERIALS AND METHODS

Silver NPs were obtained by reducing of silver nitrate with the addition of sodium citrate.[31] In brief, aqueous solution of silver nitrate (9 mg of $AgNO_3$ per 100 ml of deionized water) was heated to boil. Then, 2.5 ml of 1% sodium citrate solution was added drop by drop under intensive stirring to the above silver nitrate solution. During the synthesis process, the solution became a yellow-green color, which is typical nature of silver colloidal NPs. As a result, a 10^{-7} mol/L concentration of silver NPs was obtained. The method for determining the concentration of the silver NPs in a solution is described in detail in Reference 32.

Tetraethyl orthosilicate (99.8%, Sigma Aldrich), ammonium hydroxide (NH_4OH, ACS reagent 28.0%–30% NH_3) and dehydrated ethanol were added to the above synthesized silver nanoparticle solution to produce the $Ag@SiO_2$ core-shell nanostructures. In this synthesis, silver NPs were transferred from an aqueous solution to an isopropyl alcohol before the synthesis of the SiO_2 shells.

The average sizes of NPs and NSs were determined by the method of dynamic light scattering on the Zetasizer Nano ZS particle size analyzer (Malvern).

ITO (Indium Tin Oxide) coated glass substrates were used to assemble solar cells. The ITO glasses (2×2 cm) previously etched by one-third were successively washed in a surfactant solution, and in deionized water. Next, the dried substrates were sonicated in both acetone (20 min) and isopropyl alcohol (IPA) (15 min) separately. Finally, the ITO surfaces were treated in oxygen plasma cleaner (PC-002-CE, Harrick Plasma).

An aqueous solution of PEDOT:PSS (PH 1000, M122, Ossila) was used in the PSC. To increase the conductivity of the film, additional solvents such as dimethylsulfoxide (DMSO) and isopropyl alcohol were added to the PEDOT:PSS solution.

A spin-coating equipment (SPIN 150i, Netherlands) was used to deposit the PEDOT:PSS solution onto the glass surface. For the film deposition, 40 μl of the PEDOT:PSS solution with all additives was spinned onto ITO substrate at either 1000 rpm or 4500 rpm. The films were further annealed at 110°C for 30 min.

A four-probe measurement method was applied to determine the surface electrical resistance of the obtained composite films (ρ).

Concentration of additional solvents was determined to obtain the minimum surface resistance of the polymer films. The IPA solution of $Ag@SiO_2$ was added to the PEDOT:PSS solution with additives. The optimal concentration of the additional solvents was achieved by adding various concentrations of $Ag@SiO_2$ NS.

A chlorobenzene solution of P3HT:PC60BM [e.g. poly (3-hexylthiophene-2,5-diyl and [6,6]-phenyl-C60-butyric acid methyl ester or 10 mg P3HT, 8 mg PC60BM in 1 mL of chlorobenzene] was prepared to deposit as the photoactive layer. Also the P3HT:PC60BM films were prepared with the addition of $Ag@SiO_2$ NSs in the range of 10^{-10} mol/L and 10^{-8} mol/L. Sixty microliters of the finished solution was spin-coated onto substrate in an inert atmosphere under the following conditions: 500 rpm—30 s, 700 rpm—120 s. The films were further annealed at 80°C for 30 min.

The thickness of the produced polymer films were determined using a scanning electron microscope (SEM) Tescan Mira 3. The thickness of films was 300 nm for the PEDOT:PSS films obtained at a rotation speed of 1000 rpm and 90 nm at a rotation speed of 4500 rpm. The P3HT:PCBM films thickness averaged 150 nm.

InGa eutectic material (Sigma-Aldrich) was used as the upper electrode to assemble the PSC.

The absorption spectra of the various PSC layers were measured by Cary 300 spectrophotometer (Agilent).

The fluorescence lifetime was measured by the time–correlated photon counting method at the following excitation condition ($\lambda_{gen} = 532$ nm, $\tau = 120$–180 ps, Becker&Hickl GmbH).[33] The fluorescence decay curves were analyzed using the SPCImage software.[34] The lifetime of the emission was determined using the following formula, which used to approximate the decay kinetics[35]:

$$I(t) = \sum_{i=1}^{3} A_i e^{\frac{t}{\tau_i}} \quad (1)$$

where τ_i, A_i are the lifetime and amplitude of each dye luminescence component $\left(\sum_{i=1}^{3} A_i = 100\%\right)$. The average lifetime of the emission was determined by the formula $\tau_\Sigma = \sum_{i=1}^{3} A_i \tau_i$.

A certified silicon cell (National Renewable Energy Laboratory, Certificate number 1239.02) was used as the reference cell for determination of an external quantum efficiency of the PSCs.

The impedance of the cells was measured using the Z 500PRO impedance meter in the potentiostatic mode at a given constant potential. The measurement method was described in Reference 36–39. To determine the main parameters of the solar cell chain, the EIS–analyzer program was used.

The current–voltage characteristics (CVC) and efficiency of solar cells were determined by a standardized solar simulator Solar Cell IV Measurement (Photo Emission Tech., Inc.) under standard 1 sun light irradiation (xenon lamp with power density of 100 mW/cm^2, Class AAA) (Figure 1).

3 | RESULTS AND DISCUSSION

In the PSC, like other solar cells the conversion process of the solar light into electrical energy consists of several major steps. They are light absorption, exciton migration to the center of charge carrier separation, charge carrier separation at the interface of P3HT:PCBM, and transport of charge carriers to counter electrodes. To improve the PSC efficiency, based on the hypothesis described in the introduction section, the core-shell nanostructures of silver (core) and silica (shell) NSs were fabricated to investigate their effect on the light transformation into the electrical energy.

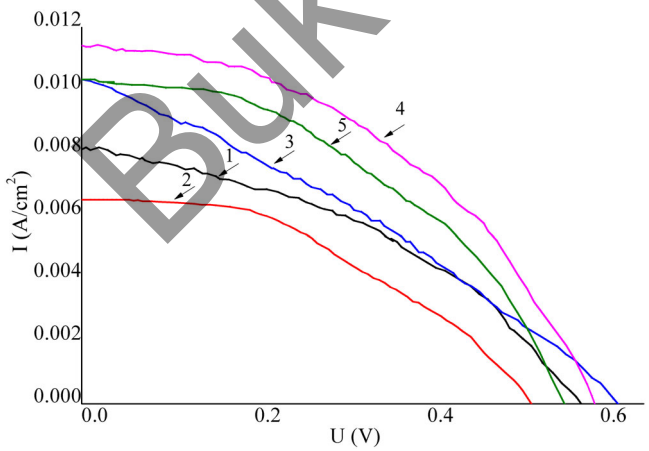

FIGURE 1 Current–voltage characteristics (CVC) of the solar cells with Ag@SiO$_2$ NSs in different layers of the cells. The CVC results (1-5) are also listed in the first and second columns of Table 2

As described in the experimental section, silver NPs were synthesized first. Average size of the silver NPs was ~5 nm (Figure S1a, [Supporting Information]). Then, the core-shell of Ag@SiO$_2$ was produced. Its average diameter was around 15 nm (Figure S1b). The shell thickness was approximately 10 nm. The absorption spectra (-Figure S2) is another indicator to monitor formation of "core-shell" NSs. The presence of the SiO$_2$ shell leads to a long-wave shift relative to the plasmonic spectra of the silver NPs. This indicates the formation of the "core-shell" NSs.[40] The shift of the spectrum is associated with a change in the dielectric characteristics of the medium surrounding the silver NPs.[40] The final concentration of Ag@SiO$_2$ NSs prepared in isopropyl alcohol solvent was equal to 4.1×10^{-8} mol/L.

Electron microscope image of the Ag@SiO$_2$ confirmed the formation of core-shell nanostructures (Figure S3).

To produce the low resistant PEDOT:PSS films, effect of additional solvents (DMSO and IPA) on the surface resistance of PEDOT:PSS films was investigated (Table S1). The results showed that the low resistance of the films were observed respectively as the volume of DMSO reached 15 volume % of the entire solution of PEDOT:PSS and as the volume IPA reached 50% of PEDOT:PSS aqueous solution. The detailed results are not shown in this article. The deposition speed of the solutions used was in the range of 1000 rpm and 4500 rpm (Table 1).

To investigate influence of core-shell structures (Ag@SiO$_2$) on the PSC performance, Ag@SiO$_2$ in IPA was added to the resulting PEDOT:PSS solution. The concentration of DMSO and IPA in the resulted solution was maintained at 15% and 50%, respectively. The final surface resistances of PEDOT:PSS films with and without Ag@SiO$_2$ NSs, are shown in Table 1. The lower resistance was

TABLE 1 Surface resistance (ρ) of the films on concentration of Ag@SiO$_2$ NSs in a mixture of PEDOT:PSS solution with 15% of DMSO and 50% of IPA

Changing conditions for the samples	ρ (kΩ/sq.)
4500 rpm without NSs	352.66
4500 rpm C(Ag@SiO$_2$) = 10^{-10} mol/L	70.48
4500 rpm C(Ag@SiO$_2$) = 10^{-9} mol/L	47.16
4500 rpm C(Ag@SiO$_2$) = 10^{-8} mol/L	34.04
4500 rpm C(Ag@SiO$_2$) = 10^{-7} mol/L	15.25
1000 rpm without NSs	147.52
1000 rpm C(Ag@SiO$_2$) = 10^{-10} mol/L	9.18
1000 rpm C(Ag@SiO$_2$) = 10^{-9} mol/L	6.86
1000 rpm C(Ag@SiO$_2$) = 10^{-8} mol/L	0.23
1000 rpm C(Ag@SiO$_2$) = 10^{-7} mol/L	1.34

obtained for PEDOT:PSS films with NSs at C(Ag@SiO_2) = 10^{-8} mol/L deposited at 1000 rpm relative to the resistance of the film without the core-shell NS. The decrease in the surface resistance of PEDOT:PSS is dependent on the electrostatic interaction between Ag@SiO_2 NSs and PEDOT and PSS.[25]

Thus, the addition of Ag@SiO_2 NSs with a SiO_2 dielectric shell leads to a decrease in the electrical resistance of PEDOT:PSS films. The similar results were found previously for the film with the addition of Ag@TiO_2 NS.[36] The electrical resistance of PEDOT:PSS films with additive of Ag@TiO_2 NSs was lower than the resistance of the films with silver nanoparticles.

An increase in conductivity was observed upon the addition of SiO_2 nanoparticles to PEDOT films[41] and an increased conductivity in hybrid PEDOT–SiO_2 films.[42] The increase in the conductivity of the PEDOT films in the presence of SiO_2 nanoparticles was explained by the formation of a conducting molecular complex between PEDOT and SiO_2[43] or by a change in the structural organization of PEDOT polymer chains in the presence of SiO_2 nanoparticles.[23] Analysis of absorption spectra showed the absence of an additional band at 500–1200 nm in the absorption spectra of PEDOT:PSS + Ag@SiO_2 composite films (Figure 2, curves 3–6), associated with the formation of a charge transfer complex PEDOT and SiO_2.[25] Therefore, a more likely mechanism leading to an increase in the conductivity of PEDOT:PSS films in the presence of Ag@SiO_2 NS is a change in the structural organization of PEDOT polymer chains in the presence of SiO_2, which was observed in Reference 25.

The PSCs with addition of various concentration of Ag@SiO_2 NSs in the PEDOT:PSS layer and in the P3HT:PCBM layer were respectively studied (Figure 1). It was found that the efficiency of the PCSs with addition of Ag@SiO_2 NSs in the photoactive layer (P3HT:PCBM) was smaller than the efficiency of cells without NSs for all concentration range of Ag@SiO_2 NSs (Table 2). On the contrary, the PSC efficiency with addition of Ag@SiO_2 NSs in the PEDOT:PSS layer showed relatively better performance except the PSC cell with 10^{-10} mol/L of

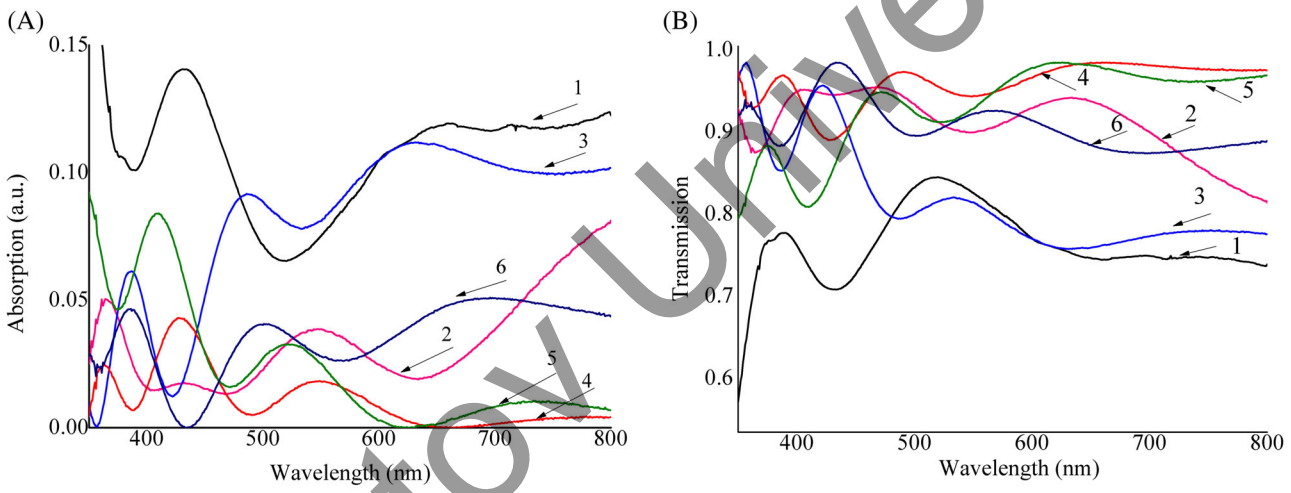

FIGURE 2 Absorption (A) and transmission (B) spectra of films: 1—glass substrate with ITO coating; 2—PEDOT:PSS without NSs; 3—PEDOT:PSS with NSs, C(Ag@SiO_2) = 10^{-10} mol/L; 4—PEDOT:PSS, C(Ag@SiO_2) = 10^{-9} mol/L; 5—PEDOT:PSS, C(Ag@SiO_2) = 10^{-8} mol/L; 6—PEDOT:PSS, C(Ag@SiO_2) = 10^{-7} mol/L

TABLE 2 Photovoltaic parameters of PSCs with different location and concentration of Ag/SiO_2 NSs

Sample	J_{SC} (mA/cm^2)	U_{OC} (V)	FF	η (%)	R_{SH} (kΩ/cm^2)	R_{SER} (mΩ/cm^2)	S (cm^2)
Cell without NSs additives (**1**)	8.18	0.571	0.41	1.91	1.52	0.12	0.12
NSs in the active layer P3HT:PCBM, C(Ag@SiO_2) = 10^{-10} mol/L	5.38	0.495	0.50	1.34	0.55	0.03	0.1
NSs in the active layer P3HT:PCBM, C(Ag@SiO_2) = 10^{-9} mol/L (**2**)	6.38	0.509	0.54	1.75	2.40	–	0.04
NSs in the active layer P3HT:PCBM, C(Ag@SiO_2) = 10^{-8} mol/L	7.08	0.431	0.38	1.17	11.25	0.02	0.05
NSs in PEDOT:PSS, C(Ag@SiO_2) = 10^{-10} mol/L	14.48	0.159	0.26	0.60	4.70	0.22	0.05
NSs in PEDOT:PSS, C(Ag@SiO_2) = 10^{-9} mol/L (**3**)	10.38	0.609	0.31	1.98	1.38	0.10	0.06
NSs in PEDOT:PSS, C(Ag@SiO_2) = 10^{-8} mol/L (**4**)	11.4	0.586	0.46	3.05	4.3	0.03	0.08
NSs in PEDOT:PSS, C(Ag@SiO_2) = 10^{-7} mol/L (**5**)	10.2	0.559	0.46	2.54	2.3	0.01	0.06

Ag@SiO_2. Furthermore, the PSCs were tested via changing concentration of Ag@SiO_2 NSs from 10^{-10} mol/L to 10^{-7} mol/L in the PEDOT:PSS layers (Table 2). The PSC with 10^{-8} mol/L of Ag@SiO_2 showed the best result among all concentrations of Ag@SiO_2 NS in the PEDOT:PSS layer.

The efficiency of the PSC cell as the concentration of Ag@SiO_2 NSs was 10^{-10} mol/L in PEDOT:PSS showed 3 times as low as the efficiency of cells without Ag@SiO_2 NSs (Table 2). As the concentration of NSs is equal to 10^{-9} mol/L, the efficiency reached that of the cells without NPs. Further increase of the concentration (C (Ag@SiO_2) = 10^{-8} mol/L) results in the increase of the PCSs efficiency by 60% compared to the cells without Ag@SiO_2 NSs. Decrease of the surface resistance in the PEDOT:PSS films was observed for the cell with C(Ag@SiO_2) = 10^{-8} mol/L (Table 1).

Absorption and transmission spectra of the ITO coated glass substrate and PEDOT:PSS films with inclusion of different concentration of Ag@SiO_2 NSs are shown in Figure 2. The glass substrate with ITO coating contributes more to light absorption than that of PEDOT:PSS films with Ag@SiO_2 NSs (Figure 2B). An increase of the Ag@SiO_2 NS concentration in the PEDOT:PSS films does not lead to significant absorption of light in this films.

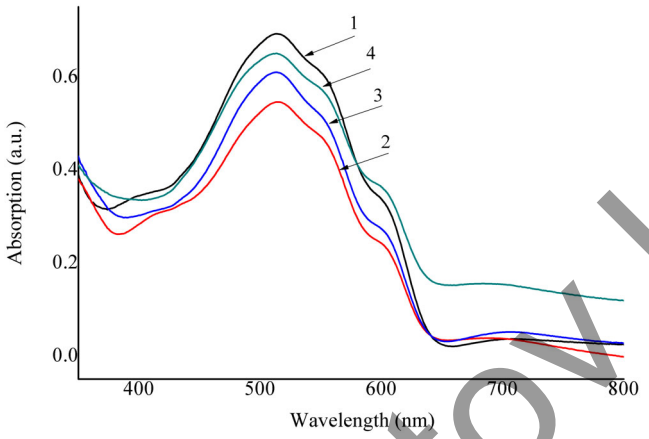

FIGURE 3 Absorption spectra of P3HT:PCBM films on the surface of PEDOT:PSS films: 1—PEDOT:PSS without NSs; 2—PEDOT:PSS with NSs, C(Ag@SiO_2) = 10^{-10} mol/L; 3—PEDOT:PSS, C(Ag@SiO_2) = 10^{-9} mol/L; 4—PEDOT:PSS, C(Ag@SiO_2) = 10^{-8} mol/L

Absorption spectra of the P3HT:PCBM layers on the surface of PEDOT:PSS films without and with Ag@SiO_2 NSs are shown in Figure 3. Addition of Ag@SiO_2 NSs does not significantly reduce absorbance of P3HT:PCBM films. Optical density (*D*) of the P3HT:PCBM active layer varies from 0.54 for PSC with C (Ag@SiO_2) = 10^{-10} mol/L to $D = 0.69$ for PSC without Ag@SiO_2 NSs, which corresponds to 8% of change in the light absorption efficiency of the P3HT:PCBM layer. The shape of the absorption spectra and the ratio of intensities for the ordered and disordered phases of P3HT polymer indicate a small effect of Ag@SiO_2 NSs in PEDOT:PSS films on the degree of ordering of the P3HT polymer.

Temporal properties for the exciton migration to the charge carrier separation center were estimated from a luminescence curve of the P3HT film in the PSC.[26] The luminescence kinetics of the polymer film demonstrated a non-exponential decay. The time related parameters were obtained from the kinetic curve of the luminescence using a two exponent equation (Table 3). The first component of the kinetics is a lifetime of $\tau_1 = 0.12$ ns, which is about 97% of integral intensity of the emission. The estimated lifetime is equal to the duration of the laser pulse, indicating that the duration of the photoprocesses is shorter than the duration of the laser photoexcitation pulse. The second component τ_2 is about 2.5% of the integral emission. The addition of Ag@SiO_2 NSs to the PEDOT:PSS films leads to only a decrease in the luminescence lifetime τ_2 (Table 3). A comparison of the data obtained for the luminescence of P3HT in PSCs with the data for the P3HT polymer film on the glass surface shows that the τ_2 for the luminescence of the polymer in PSCs can be associated with luminescence from isolated P3HT chains or a recombination luminescence when an electron is returned to polymer chain from the PCBM. The low value of τ_1 and its high portion in the integral luminescence shows a high probability of the exciton reaching the P3HT:PCBM interface and effective interface separation of charge carriers. Thus, the kinetics of polymer fluorescence in PSCs shows a high efficiency of the charge carrier separation process and does not show significant differences in exciton transport in the polymer of cells without and with Ag@SiO_2 NSs.

TABLE 3 Effect of Ag@SiO_2 NSs on the time characteristics of the luminescence of P3HT films on the glass surface and in PSCs

Sample	τ_Σ (ns)	τ_1 (ns)	τ_2 (ns)	A_1 (%)	A_2 (%)
P3HT films on the glass surface					
P3HT without impurities	0.30	0.22	0.30	1.8	98.2
P3HT with the addition Ag@SiO_2 NSs, C(Ag@SiO_2) = $8{\cdot}10^{-10}$ mol/L	0.23	0.18	0.45	87.3	12.7
P3HT with Ag@SiO_2 NSs, C(Ag@SiO_2) = $12{\cdot}10^{-8}$ mol/L	0.24	0.13	0.34	57.5	42.5
P3HT in PSC					
ITO – PEDOT:PSS–P3HT:PCBM	0.13	0.12	0.714	97.7	2.3
ITO – PEDOT:PSS + NSs Ag@SiO_2–P3HT:PCBM, C(Ag@SiO_2) = 10^{-10} mol/L	0.13	0.12	0.594	97.3	2.7
C(Ag@SiO_2) = 10^{-9} mol/L	0.13	0.12	0.592	97.4	2.6
C(Ag@SiO_2) = 10^{-8} mol/L	0.13	0.12	0.599	97.4	2.6

Dark current–voltage characteristics for the PSCs are shown in Figure S4. A minimum value of the reverse current in the cell is observed for 10^{-9} mol/L of Ag@SiO_2 NSs in the PEDOT:PSS layer. This indicates the minimum value of the charge carrier recombination at this concentration of Ag@SiO_2 NSs in the PEDOT:PSS. A further increase of Ag@SiO_2 NSs concentration in PEDOT:PSS to 10^{-8} mol/L leads to a slight increase in the forward and reverse current in the cell, which indicates an increase in the recombination rate of charge carriers compared to the cell with C(Ag@SiO_2) = 10^{-9} mol/L.

Effect of the LSPR on the charge carrier generation in P3HT:PC60BM was determined after measurements of external quantum efficiency of PSCs. The high external quantum efficiency indicates better charge carrier separation in P3HT:PCBM layers (Figure 4). A change in the external quantum efficiency curve (IPCE—incident photon-to-electron conversion efficiency) was observed for the Ag@SiO_2 NSs additives (Figure 4, curve 2 and 3). The increase of the IPCE value was found for the concentration of C (Ag@SiO_2) = 10^{-8} mol/L. Furthermore, the curve 3 in Figure 5 shows the difference in the spectrum, which indicates the increase of IPCE from 400 nm to 520 nm. Both absorption spectra and IPCE curve of the cells consisting of all functional layers (glass substrate with ITO, PEDOT:PSS film with NSs and layer P3HT:PC60BM) were measured to determine influence of PEDOT:PSS composite films with/without Ag@SiO_2 NSs to the PSC cells. Absorption spectra of the PEDOT:PSS films with C(Ag@SiO_2) = 10^{-8} mol/L show the presence of absorption bands at 407, 520 and 730 nm (Figure 2, curve 5). For the PEDOT:PSS films without NSs the absorption bands at 407 and 730 nm are not observed (Figure 2, curve 2).

To explain the results, the extinction, absorption and scattering spectra of Ag NPs in media with different values of the real part of the dielectric permittivity of the medium were simulated by the program Mieplot (V. 4.6.11). The algorithm of numerical calculations is described in Reference 44. For the calculations, the size of the silver NPs used was ~5 nm. The actual permittivity of PEDOT:PSS (ε_m = 2.25) was taken from the Reference 45. The results of spectrum modeling are shown in Figures 5 and 6.

The comparison of the spectra shows that the increase in the quantum efficiency of the cells (IPCE) is associated with the LSPR effect of Ag@SiO_2 NSs, which can be initiated either by an increase of the light absorption or by an increase of light scattering in the cells. The enhanced light scattering can lead to an increase in the optical path of light, in the absorption of these light bands, and in the generated charge carriers. At the same time, the value of the scattering cross-section of the Ag NPs is 3.5 times as high as the value of the absorption cross-section of the Ag NPs (Figure 6). As far as silver nanoparticles with a size of 5 nm are concerned, light scattering prevails over absorption. The spectral-difference spectrum of the IPCE which are consistent with the calculated extinction and scattering spectra of the Ag NPs, indicates that the scattering leads to an increase in the IPCE value of the cells.

The effect of LSPR of Ag@SiO_2 NSs on the process of charge carrier generation in PSCs showed the high quantum efficiency for the charge carrier generation. Comparison of IPCE spectra with the absorption spectra of PEDOT:PSS films with Ag@SiO_2 NSs and the

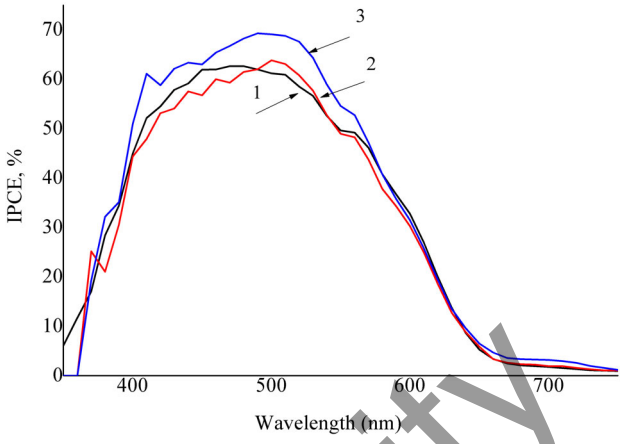

FIGURE 4 IPCE spectra of solar cells without and with NSs: 1—cell without NSs; 2—PEDOT:PSS + Ag@SiO_2 NSs, C(Ag@SiO_2) = 10^{-9} mol/L; 3—PEDOT:PSS, C(Ag@SiO_2) = 10^{-8} mol/L

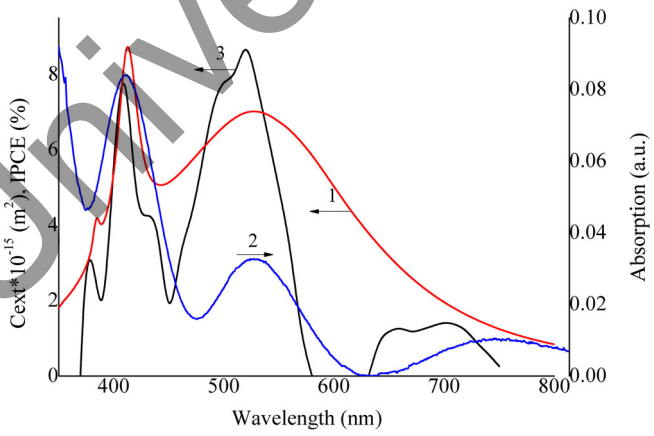

FIGURE 5 Extinction spectra of silver NPs with d = 5 nm and ε_m = 2.25 (1), absorption of PEDOT:PSS film with C(Ag@SiO_2) = 10^{-8} mol/L (2), and the difference spectrum of IPCE (curve 1, Figure 4)—IPCE (curve 3, Figure 4) (3)

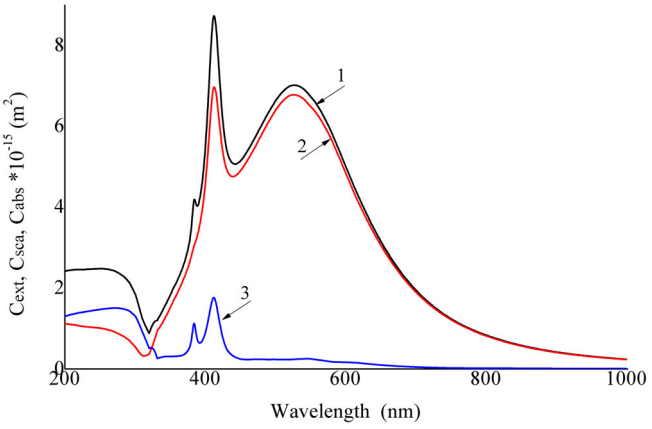

FIGURE 6 Calculated extinction (1), scattering (2), and absorption (3) spectra of Ag NPs in medium with permittivity ε_m = 2.25

results of the simulation of the extinction spectra showed the predominant effect of light scattering by Ag NPs on the IPCE of the cells.

Influence of LSPR on the recombination and transport of charge carriers for the PSCs was likewise studied by the impedance spectra (Figure 7) according to the procedure given in the work of Bisquit and co-authors.[38] The electrical circuits used for the analysis of the cells are shown in Figure S5 (Supporting Information). The electrical model (Figure S5c) used an equivalent circuit that contains a series resistor R1 to account for the resistance between the ITO and the wires in the PSCs. The bimolecular recombination of electrons and holes is modeled by resistive elements (R3 and R4). The distributed chemical capacity $CPE_T = C\mu$ is described using a constant phase element (CPE1). The resistance to electron transport in the cell is described using the resistor R2. The capacitance $C_1 \approx \varepsilon_0\varepsilon_m A/L$ is the dielectric contribution of the diode, *A* is the area, *L* is the thickness of the diode.

The described impedance model contains two characteristic times associated with electron diffusion $\tau_d = R2{\cdot}CPE_T$ (time of flight) and the effective lifetime $\tau_n = R3{\cdot}CPE_T$, in accordance with the models shown in Figure S5.[35]

The results of the circuit elements obtained are shown in Table 4. Addition of 10^{-9} mol/L of $Ag@SiO_2$ NSs to PEDOT:PSS increases the resistance of all resistive elements from R1 to R4. A further increase of the concentration of $Ag@SiO_2$ NSs dwindled cell resistances of R1, R3, and R4 to the original value. While R2 value for the cell consisting of PEDOT:PSS and 10^{-8} mol/L of $Ag@SiO_2$ is 30% lower than the R2 resistance for the cells without NSs, this is not fully consistent with the dark surface resistance data for PEDOT:PSS films with $Ag@SiO_2$ NSs. The surface resistance of the films with 10^{-9} mol/L of $Ag@SiO_2$ obtained at 1000 rpm is 8.7 times smaller than the resistance of the PEDOT:PSS films with 10^{-8} mol/L of $Ag@SiO_2$.

The diffusion times, effective lifetimes, and mobility of charge carriers are shown in Table 5. Initially, addition of $Ag@SiO_2$ NS in PEDOT:PSS leads to an increase in the diffusion time and effective lifetime of charge carriers in PSCs. At 10^{-8} mol/L of $Ag@SiO_2$ the values are closer to the values of τ_d and τ_n of the cell without NSs. The results obtained for the samples with $C(Ag@SiO_2) = 10^{-9}$ mol/L and 10^{-8} mol/L in PEDOT:PSS was not applicable for the chosen electrical circuits shown in Figure S5a or b schemes. The scheme (c) in Figure S5 was used for the samples with 10^{-9} mol/L and 10^{-8} mol/L of $Ag@SiO_2$. The reason for using scheme (c) is the presence of two recombination times in the cell with $Ag@SiO_2$ NS (Table 5). This, in turn, may be due to the different effects of $Ag@SiO_2$ NSs on the solar cells.

Thus, the performed studies allowed us to determine the concentrations of $Ag@SiO_2$ NS s in PEDOT:PSS, at which there is a minimal resistance to the charge carriers transport in PEDOT:PSS films is observed. Results obtained through impedance spectroscopy of our PSCs are consistent with or supported the results from the optical investigation and current–voltage measurements of the cells.

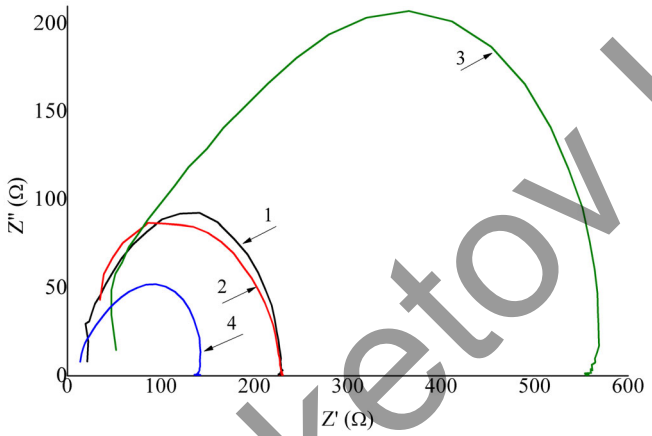

FIGURE 7 Impedance spectra in Nyquist coordinates of PSCs without NSs (1) and with NSs (2–4): (2) PEDOT:PSS with NSs, $C(Ag@SiO_2) = 10^{-10}$ mol/L; (3) $C(Ag@SiO_2) = 10^{-9}$ mol/L; (4) $C(Ag@SiO_2) = 10^{-8}$ mol/L

TABLE 5 Effect of Ag/SiO_2 NSs on electric transport (τ_d, μ) and recombination characteristics (τ_{n1}, τ_{n2}) in polymer cells

Sample	τ_d (μs)	μ ($cm^{-3}\ V^{-1}\ s^{-1}$)	τ_{n1} (μs)	τ_{n2} (μs)
ITO – PEDOT:PSS–P3HT:PCBM	7.5	1.3	11	–
ITO – PEDOT:PSS + $Ag@SiO_2$ NSs – P3HT:PCBM $C(Ag@SiO_2) = 10^{-10}$ mol/L	39.8	0.24	13	–
$C(Ag@SiO_2) = 10^{-9}$ mol/L	14.2	0.68	76	37
$C(Ag@SiO_2) = 10^{-8}$ mol/L	6.5	1.5	16.5	15

TABLE 4 Values of circuit elements of solar cells with $Ag@SiO_2$ NSs

Sample	L_1 (μH)	R_1 (Ω)	R_2 (Ω)	R_3 (Ω)	R_4 (Ω)	C_1. (nF)	CPE_T (nF)	CPE_P	L_1 (10^{-16} H)	Equivalent circuits (Figure S5)
ITO – PEDOT:PSS – P3HT:PCBM	2.3	12	88	130	–	1.7	85	0.94	–	(a)
ITO – PEDOT:PSS + $Ag@SiO_2$ NSs – P3HT:PCBM, $C(Ag@SiO_2) = 10^{-10}$ mol/L	–	18	160	54	–	5.5	249	0.88	7	(b)
$C(Ag@SiO_2) = 10^{-9}$ mol/L	–	37	194	1038	508	9.2	73	0.95	7	(c)
$C(Ag@SiO_2) = 10^{-8}$ mol/L	–	12	59	150	140	22	110	0.98	7	(c)

4 | CONCLUSION

LSPR effect of $Ag@SiO_2$ NS on the conversion of light into electrical energy for the polymer solar cells (based on P3HT:PCBM) was studied. Inclusion of $Ag@SiO_2$ NS in PSC eliminates influence of metal NPs for electron transfer between the polymer and the metal NPs. Through study of the PEDOT:PSS film surface resistance by adding $Ag@SiO_2$ NSs, it was found that the lowest resistance was observed for PEDOT:PSS films with 10^{-8} mol/L of $Ag@SiO_2$ NSs deposited at 1000 rpm.

In contrast to the absorption spectra for the glass with the ITO film, the addition of $Ag@SiO_2$ NSs into the PSC does not significantly weaken the light flux passing through the PEDOT:PSS polymer films or the P3HT:PCBM active layer.

Kinetic study of polymer fluorescence in the PSCs showed a high efficiency of the charge carrier separation and does not show significant differences in exciton transport in the polymer of cells with Ag/SiO_2NSs.

Sixty percent of increase in the efficiency of polymer solar cells was registered for the optimal concentration of $Ag@SiO_2$ NSs, 10^{-8} mol/L, in PEDOT:PSS film. The enhanced efficiency of the polymer solar cell is ascribed to a decrease of the electrical resistance of the PEDOT:PSS layer with addition of $Ag@SiO_2$ NSs. The increased absorptivity in the polymer is the result of light scattering on $Ag@SiO_2$ NSs.

Addition of $Ag@SiO_2$ in PEDOT:PSS with concentrations of 10^{-10} and 10^{-9} mol/L leads to a decrease in the mobility of charge carriers in polymer cells. As the concentration of $Ag@SiO_2$ in the PEDOT:PSS film is 10^{-8} mol/L, the mobility of charge carriers in the film surpass the values for the cell without NSs.

ACKNOWLEDGMENTS

The authors express their gratitude to Mr. Marat Nuraje from ERMHS for editing and proof-reading the whole manuscript. This work was supported partially by FDRG grant of Nazarbayev University (SEDS2020 016).

CONFLICT OF INTEREST

The authors declare that the research was conducted in the absence of any commercial or financial relationships that could be construed as a potential conflict of interest.

DATA AVAILABILITY STATEMENT

The data that support the findings of this study are available from the corresponding author upon reasonable request.

ORCID

Nurxat Nuraje https://orcid.org/0000-0002-4335-8905

REFERENCES

1. Bhongale CJ, Chaudhari R. All-organic solution processed solar cells based on terephthaladehyde self-assembled monolayer. *Eng Sci*. 2021;15:89-94.
2. Lin Y, Firdaus Y, Nugraha MI, et al. 17.1% efficient single-junction organic solar cells enabled by n-type doping of the bulk-heterojunction. *Adv Sci*. 2020;7(7):1903419.
3. Bulavko GV, Ishchenko AA. Organic bulk heterojunction photovoltaic structures: design, morphology and properties. *Russ Chem Rev*. 2014;83(7):575-599.
4. Mahadik SA, Patil A, Pathan HM, Salunke-Gawali SS, Butcher RJ. Thionaphthoquinones as photosensitizers for TiO2 nanorods and ZnO nanograin based dye-sensitized solar cells: effect of nanostructures on charge transport and photovoltaic performance. *Eng Sci*. 2020;14:46-58.
5. Ibrayev N, Omarova G, Seliverstova E, Alex A, Ishchenko E, Nuraje N. Plasmonic effect of Ag nanoparticles on polymethine dyes sensitized titanium dioxide. *Eng Sci*. 2021;14:69-77.
6. Bade BR, Rondiya SR, Kore KB, et al. Room temperature synthesis of formamidinium lead iodide (FAPbI3) perovskite for low-cost absorber in solar cells. *ES Energy Environ*. 2021;13:31-36.
7. Jathar SB, Rondiya SR, Bade BR, et al. Facile method for synthesis of CsPbBr3 perovskite at room temperature for solar cell applications. *ES Mater Manuf*. 2021;12:72-77.
8. Kamat PV. Photophysical, photochemical and photocatalytic aspects of metal nanoparticles. *J Phys Chem B*. 2002;106(32):7729-7744.
9. Chin SF, Pang SC, Dom FEI. Sol-gel synthesis of silver/titanium dioxide (Ag/TiO2) core-shell nanowires for photocatalytic applications. *Mater Lett*. 2011;65(17):2673-2675.
10. Hentschel M, Utikal T, Giessen H, Lippitz M. Quantitative modeling of the third harmonic emission spectrum of plasmonic nanoantennas. *Nano Lett*. 2012;12(7):3778-3782.
11. Walsh GF, Dal Negro L. Enhanced second harmonic generation by photonic–plasmonic fano-type coupling in nanoplasmonic arrays. *Nano Lett*. 2013;13(7):3111-3117.
12. Lal S, Link S, Halas NJ. Nano-optics from sensing to waveguiding. *Nat Photon*. 2007;1(11):641-648.
13. Khodashenas B, Ghorbani HR. Synthesis of silver nanoparticles with different shapes. *Arab J Chem*. 2019;12(8):1823-1838.
14. Khlebtsov NG. Optics and biophotonics of nanoparticles with a plasmon resonance. *Quantum Electron*. 2008;38(6):504-529.
15. Chaudhuri RG, Paria S. Core/shell nanoparticles: classes, properties, synthesis mechanisms, characterization, and applications. *Chem Rev*. 2012;112(4):2373-2433.
16. Cheng H, Lu Z, Gao Q, et al. PVDF-Ni/PE-CNTs composite foams with co-continuous structure for electromagnetic interference shielding and photo-electro-thermal properties. *Eng Sci*. 2021;16:1-10. doi:10.30919/es8d518
17. Yan H, Dai X, Ruan K, et al. Flexible thermally conductive and electrically insulating silicone rubber composite films with BNNS@Al2O3 fillers. *Adv Compos Hybrid Mater*. 2021;4(1):36-50.
18. Sang G, Xu P, Yan T, et al. Interface engineered microcellular magnetic conductive polyurethane nanocomposite foams for electromagnetic interference shielding. *Nano-Micro Lett*. 2021;13(1):153.
19. Zhao S, Pei L, Li H, et al. Research progress in toughening modification of polybenzoxazine. *Eng Sci*. 2020;14:14-26.
20. Chan K, Wright M, Elumalai N, Uddin A, Pillai S. Plasmonics in organic and perovskite solar cells: optical and electrical effects. *Adv Opt Mater*. 2017;5(6):1600698.
21. Shin J, Song M, Hafeez H, et al. Harvesting near- and far-field plasmonic enhancements from large size gold nanoparticles for improved performance in organic bulk heterojunction solar cells. *Org Electron*. 2019;66:94-101.
22. Kukhta A, Kolesnik E, Ritchik D, Galkin V, Zholnerevich I. A numerical analysis of processes in organic electroluminescent structure with metal nanoparticles. *J Optoelectron Adv Mater*. 2004;6:405-412.
23. Lim EL, Yap CC, Mat Teridi MA, Teh CH, Yusoff AR b M, Jumali MHH. A review of recent plasmonic nanoparticles incorporated P3HT: PCBM organic thin film solar cells. *Org Electron*. 2016;36:12-28.

24. Stratakis E, Kymakis E. Nanoparticle-based plasmonic organic photovoltaic devices. *Mater Today*. 2013;16(4):133-146.
25. Hu L, Song J, Yin X, Su Z, Li Z. Research progress on polymer solar cells based on PEDOT:PSS electrodes. *Polymers*. 2020;12(1):145.
26. Xu X, Kyaw AKK, Peng B, et al. A plasmonically enhanced polymer solar cell with gold–silica core–shell nanorods. *Org Electron*. 2013; 14(9):2360-2368.
27. Zhang R, Zhou Y, Peng L, et al. Influence of SiO2 shell thickness on power conversion efficiency in plasmonic polymer solar cells with Au nanorod@SiO2 core-shell structures. *Sci Rep*. 2016;6(1):25036.
28. Kim JY, Kim SH, Lee H-H, et al. New architecture for high-efficiency polymer photovoltaic cells using solution-based titanium oxide as an optical spacer. *Adv Mater*. 2006;18(5):572-576.
29. Kukhta AV, Pochtenny AE, Misevich AV, et al. Optical and electrophysical properties of nanocomposites based on PEDOT: PSS and gold/silver nanoparticles. *Phys Solid State*. 2014;56(4):827-834.
30. Ibrayev N, Serikov T, Zavgorodniy A, Sadykova A. The effect of the DSSC photoanode area based on TiO2/Ag on the conversion efficiency of solar energy into electrical energy. *IOP Conf Ser Mater Sci Eng*. 2018;289:012024.
31. Bastús NG, Merkoçi F, Piella J, Puntes V. Synthesis of highly monodisperse citrate-stabilized silver nanoparticles of up to 200 nm: kinetic control and catalytic properties. *Chem Mater*. 2014;26(9):2836-2846.
32. Ibrayev N, Ishchenko A, Afanasyev D, Zhumabay N. Active laser medium for near-infrared spectral range based on electron-unsymmetrical polymethine dye and silver nanoparticles. *Appl Phys B*. 2019;125(9):182.
33. Becker W. *The bh TCSPC handbook*. Becker & Hickle GmbH; 2019.
34. Becker W. Fluorescence lifetime imaging—techniques and applications. *J Microsc*. 2012;247(2):119-136.
35. Afanasyev D, Ibrayev N, Nurmakhanova A. Effect of spin-orbit interaction on recombination luminescence of dye in films of halogen-containing derivative poly-N-epoxypropylcarbazole. *J Photochem Photobiol A Chem*. 2020;394:112442.
36. Alikhaidarova E, Afanasyev D, Ibrayev N. Electrical properties of nanocomposite materials based on PEDOT:PSS polymer mixture doped with Ag, Ag-TiO2 and Ag-SiO2 nanoparticles. *Mater Today Proc*. 2020;25:28-32.
37. Ibrayev NK, Afanasyev DA. Electrical characteristics of semiconductor polymer. Films doped with silver nanoparticles. *Eurasian Phys Tech J*. 2018;15(2):76-82.
38. Bisquert J. Theory of the impedance of electron diffusion and recombination in a thin layer. *J Phys Chem B*. 2002;106(2):325-333.
39. Garcia-Belmonte G, Munar A, Barea EM, Bisquert J, Ugarte I, Pacios R. Charge carrier mobility and lifetime of organic bulk heterojunctions analyzed by impedance spectroscopy. *Org Electron*. 2008; 9(5):847-851.
40. Afanasyev DA, Ibrayev NK, Serikov TM, Zeinidenov AK. Effect of the titanium dioxide shell on the plasmon properties of silver nanoparticles. *Russ J Phys Chem A*. 2016;90(4):833-837.
41. Lee JS, Choi Y-J, Park H-H, Chul PJ. Electrochromic properties of poly(3,4-ethylenedioxythiophene) nanocomposite film containing SiO2 nanoparticles. *J Appl Polym Sci*. 2011;122(5):3080-3085.
42. Yim J-H. Mechanically robust poly(3,4-ethylenedioxythiophene)–SiO2 hybrid conductive film prepared by simultaneous vapor phase polymerization. *Compos Sci Technol*. 2013;86:45-51.
43. Huh P-H, Kim S-C, Kim Y-H, et al. Recovery and characterization of pure poly(3,4-ethylenedioxythiophene) via biomimetic template polymerization. *Polym Eng Sci*. 2007;47(1):71-75.
44. Grainger RG, Lucas J, Thomas GE, Ewen GBL. Calculation of Mie derivatives. *Appl Optics*. 2004;43(28):5386-5393.
45. Chen C-W, Hsiao S-Y, Chen C-Y, Kang H-W, Huang Z-Y, Lin H-W. Optical properties of organometal halide perovskite thin films and general device structure design rules for perovskite single and tandem solar cells. *J Mater Chem A*. 2015;3(17):9152-9159.

SUPPORTING INFORMATION

Additional supporting information may be found in the online version of the article at the publisher's website.

How to cite this article: Alikhaidarova E, Afanasyev D, Ibrayev N, Nuraje N. Plasmonic enhanced polymer solar cell with inclusion of Ag@SiO_2 core-shell nanostructures. *Polym Adv Technol*. 2022;33(3):1000-1008. doi:10.1002/pat.5574